

Multiple Bloch surface wave excitation with gratings

*Original*

Multiple Bloch surface wave excitation with gratings / Lewis, Asilevi; Descrovi, Emiliano; Pesonen, Henri; Roussey, Matthieu; Turunen, Jari. - In: JOURNAL OF THE EUROPEAN OPTICAL SOCIETY. RAPID PUBLICATIONS. - ISSN 1990-2573. - 20:1(2024). [10.1051/jeos/2024007]

*Availability:*

This version is available at: 11583/2986256 since: 2024-02-23T09:02:12Z

*Publisher:*

EDP Sciences

*Published*

DOI:10.1051/jeos/2024007

*Terms of use:*

This article is made available under terms and conditions as specified in the corresponding bibliographic description in the repository

*Publisher copyright*

EDP preprint/submitted version e/o postprint/Author's Accepted Manuscript

© EDP Sciences. The original publication is available at

[https://jeos.edpsciences.org/articles/jeos/full\\_html/2024/01/jeos20230066/jeos20230066.html](https://jeos.edpsciences.org/articles/jeos/full_html/2024/01/jeos20230066/jeos20230066.html)

(Article begins on next page)

# Multiple Bloch surface wave excitation with gratings

Atsu L. Asilevi<sup>1,\*</sup>, Emiliano Descrovi<sup>2</sup>, Henri Pesonen<sup>3</sup>, Matthieu Roussey<sup>1</sup>, and Jari Turunen<sup>1</sup>

<sup>1</sup>Center for Photonics Sciences, Department of Physics and Mathematics, University of Eastern Finland, P.O. Box 111, 80101 Joensuu, Finland

<sup>2</sup>Dipartimento di Scienza Applicata e Tecnologia, Politecnico di Torino, 10129 Torino, Italy

<sup>3</sup>Dispelix Oy, Yliopistokatu 7, FI-80130 Joensuu, Finland

\*Corresponding author: lewisa@uef.fi

**Abstract.** We study the coupling of a finite number of Bloch surface waves (BSWs) propagating in different directions at the surface of a dielectric multilayer. These surface waves arise from a set of diffraction orders associated to a grating on the bottom surface of the substrate that is illuminated by a normally incident beam. Simultaneous excitation of multiple BSWs is possible with a set of diffraction orders having the same radial spatial frequency. Using rigorous electromagnetic theory, we design gratings for simultaneous excitation of two, four and six BSWs propagating in directions separated by  $\pi$ ,  $\pi/2$  and  $\pi/3$  azimuthal intervals, respectively.

**Keywords:** Evanescent waves, Surface Electromagnetic Waves, Bloch Surface Waves, Multiple Bloch Surface Waves, MBSWs.

## 1 Introduction

Surface Electromagnetic Waves (SEW) represent an interesting option for controlling optical signals on miniaturized chips for integrated optics and sensing applications. Surface Plasmon Polaritons (SPP) are probably the most widely known SEWs, but they exhibit inherent issues related to the ohmic losses introduced by the metallic materials involved. As an alternative, SEWs sustained by dielectric multilayers (ML) have attracted a growing interest in the past decade. This kind of SEW [1] are also referred to as Bloch Surface Waves (BSWs) [2] to highlight the role of the underlying periodic multilayer structure required for their existence. BSWs offer several advantages as compared to SPPs, such as a wide spectral tunability and low losses thanks to the large choice of transparent dielectric materials available for multilayer manufacturing. In addition, BSWs can be either TE- or TM-polarized [3,4], depending on the multilayer design. Their excitation by pulsed fields has also been recently studied numerically [5].

Being surface waves, BSWs are evanescent in the medium above the multilayer surface. The coupling with free-space radiation in a BSW-based device is therefore critical as it must provide momentum matching beyond the light-line. In most of the applications proposed so far, BSW coupling is performed by means of bulky prisms, either in Kretschmann or Otto configuration [6]. However, more sophisticated approaches have been recently implemented, involving, for example, the use of individual scatterers [7–9] or miniature prisms [10] placed onto the multilayer surface. Another promising option is represented by integrating diffraction gratings within the BSW-supporting structure [11]. This has been done mainly in two different ways: with the grating being fabricated on top of the multilayer [12–14] or buried beneath the multilayer [15]. In the first case, the multilayer is substantially planar, with the ex-

ception of the top layer, where the grating unavoidably perturbs the dispersion of the BSW mode (dielectric loading/unloading effect). In the second case, the grating is fabricated on the substrate surface prior to the multilayer deposition, which occurs on the same side. The multilayer itself results to not be perfectly planar because it (partially) conforms to the underlying corrugation. In both configurations, the BSW dispersion is altered by the presence of the grating, which may lead to some difficulties regarding the precise control of optical functions of complex, possibly resonating, BSW-based architectures.

We propose an alternative approach on diffractive coupling for BSWs, with gratings fabricated on the bottom surface of a transparent substrate having the multilayer deposited on the top surface. In particular, we explore the possibility of using two-dimensional gratings to simultaneously couple BSWs propagating in more than two directions by exploiting the momentum distribution of several diffraction orders. Once the mode dispersion of the multilayer is known, our approach facilitates BSW coupling in a controllable way, as far as wavelengths/numbers and propagation directions are concerned. The directional coupling of BSWs has been already tackled in a few previous articles [16–18], although never considered for multiple directions at once. When the optical path through the substrate is also taken into account, our approach allows a predictable control onto the coupling locations of BSWs launched in different directions.

The present paper is composed as follows. We begin, in Sec. 2, by introducing the grating-based BSW excitation principle and the assumed geometrical configuration. The theoretical framework for grating design, for which we use a rigorous technique known as the Fourier Modal Method (FMM) [19], is described in Sec. 3. The design process is analogous with the synthesis of grating-based mul-

63 tiple free-space beam splitters [20], but here we need to account  
64 for the BSW excitation conditions and the polarization state of the  
65 input wave. In Sec. 4, we first consider BSW stack design, pro-  
66 viding a ‘benchmark’ stack employed in the rest of the work, and  
67 then cover the design of linear gratings for simultaneous excitation  
68 of two counter-propagating BSWs. Such designs are extended in  
69 Sec. 5 to two-dimensional periodic gratings for excitation of either  
70 four or six BSWs propagating at  $90^\circ$  or  $60^\circ$  intervals along the  
71 stack, respectively. After a discussion presented in Sec. 6, conclu-  
72 sions are drawn in Sec. 7.

## 73 2 Excitation principle and geometry

74 Figure 1 illustrates the geometry for the simplest case of excita-  
75 tion of two counter-propagating BSWs. A flat fused silica substrate  
76 with refractive index  $n_{\text{sub}} = 1.462$ , such as a 0.5 mm or 3 mm-  
77 thick  $\text{SiO}_2$  plate, is illuminated by a normally incident monochro-  
78 matic beam (wavelength  $\lambda_0$ ) from the medium underneath (air).  
79 A linear grating, with period  $d$  of the order of  $\lambda_0$ , provided on  
80 the air-substrate surface, splits the beam into three transmitted or-  
81 ders propagating within the substrate: the zeroth order  $m = 0$  and  
82 the first diffracted orders  $m = \pm 1$ . The orders  $m = \pm 1$  propa-  
83 gate in directions  $\theta_{+1}$  and  $\theta_{-1}$  given by  $\sin \theta_{\pm 1} = \pm \lambda_0 / n_{\text{sub}} d$   
84 towards the multilayer stack on the top surface of the substrate.  
85 If  $|\theta_{\pm 1}|$  matches the Kretschmann-incidence BSW excitation an-  
86 gle  $\theta_{\text{BSW}}$  for the given wavelength and polarization state (TE  
87 or TM), two counter-propagating BSWs are generated simultane-  
88 ously. The excitation is efficient as long as the angular spectrum  
89 of each diffracted order, which defines the beam divergence, falls  
90 essentially within the (stack-dependent) BSW momentum band-  
91 width. The polarization state of illumination affects the coupling  
92 significantly; we will consider only BSW excitation in TE polar-  
93 ization, which generally requires a smaller number of stack layers  
94 than TM-polarized BSW excitation.

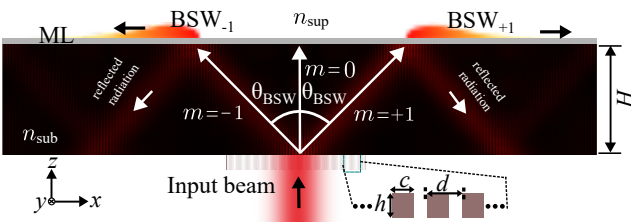


Figure 1: Principle of MBSW generation: the two-beam case. A binary linear surface-relief grating defined by period  $d$ , ridge width  $c$ , and ridge height  $h$  on the bottom of a substrate of thickness  $H$  splits the input beam into two diffracted orders  $m = -1$  and  $m = +1$ , which excite BSWs on the top surface of the substrate by interaction with the multilayer stack (ML). We assumed  $n_{\text{sub}} = 1.462$  and  $n_{\text{sup}}$  is air.

95 The parameters of the system are chosen such that the two BSWs  
96 shown in Fig. 1 are spatially separated under finite-beam illumina-  
97 tion. This feature can be useful in BSW-based platforms such as  
98 interferometers [23] and integrated components [24]. First-order  
99 diffracted beams are partially reflected at the top interface, thus  
100 propagating back into the substrate. The reflected beams continue  
101 to propagate according to multiple-reflection paths inside the sub-

strate unless they are extracted by means of diffusers or gratings.  
103 At each reflection with the ML interface, coupling to BSW occurs.  
104 Stated differently, BSWs are launched at different locations on the  
105 ML surface each time the beam is incident on the bottom interface  
106 of the dielectric stack, thus leading to the appearance of BSW inter-  
107 ference effects unless the substrate thickness  $H$  is sufficiently large  
108 to minimize spatial overlaps.

## 109 3 Theoretical framework

110 Let us consider a rectangularly periodic grating of period  $d_x \times d_y$   
111 in the cartesian  $xy$  coordinate system and assume a plane-wave  
112 illumination (at frequency  $\omega$ ) normally incident onto the substrate  
113 from air. In view of the grating equations, the wave vectors of the  
114 propagating diffraction orders  $(m, n)$  in the substrate are

$$115 \mathbf{k}_{mn} = k_{xm} \hat{x} + k_{yn} \hat{y} + k_{zmn} \hat{z} \quad (1)$$

115 where

$$116 k_{xm} = mK_x = 2\pi m/d_x, \quad (2a)$$

$$117 k_{yn} = nK_y = 2\pi n/d_y, \quad (2b)$$

$$118 k_{zmn} = \sqrt{k_0^2 n_{\text{sub}}^2 - k_{xm}^2 - k_{yn}^2}, \quad (2c)$$

116 and  $k_0 = \omega/c_0 = 2\pi/\lambda_0$  is the wave number in vacuum. After  
117 defining the radial spatial frequency of the generic order  $(m, n)$  as

$$118 k_{\rho mn} = \sqrt{k_{xm}^2 + k_{yn}^2} = \sqrt{(mK_x)^2 + (nK_y)^2}, \quad (3)$$

118 the condition  $k_{\rho mn} < k_0 n_{\text{sub}}$  identifies those diffraction orders  
119 propagating within the substrate, the others being evanescent. If  
120 we denote the refractive index of the superstrate by  $n_{\text{sup}}$  and as-  
121 sume  $n_{\text{sup}} < n_{\text{sub}}$ , order  $(m, n)$  is evanescent in the superstrate  
122 when  $k_{\rho mn} > k_0 n_{\text{sup}}$ . Considering BSW excitation, we are there-  
123 fore interested in orders with radial spatial frequencies in the range  
124  $k_0 n_{\text{sup}} < k_{\rho mn} < k_0 n_{\text{sub}}$ . We are primarily interested in the near-  
125 est neighbors of the zeroth transmitted order, while higher orders  
126 are made evanescent by appropriate choices of  $d_x$  and  $d_y$ . In the il-  
127 lustrative example presented in Fig. 2(a), orders  $(m, n) = (-1, 0)$   
128 and  $(m, n) = (+1, 0)$  fall on the yellow line of radius  $k_{\rho \text{BSW}}$ ,  
129 which defines the BSW excitation condition dictated by the ML  
130 design.

131 Following Ref. [21], we define the ‘exit plane’ of diffraction order  
132  $(m, n)$  as the plane containing the wave vector  $\mathbf{k}_{mn}$  and the unit  
133 vector  $\hat{z}$ . Further, propagation angles  $\theta_{mn}$  and  $\phi_{mn}$  of the trans-  
134 mitted orders, are defined as

$$135 k_{xm} = k_0 n_{\text{sub}} \sin \theta_{mn} \cos \phi_{mn}, \quad (4a)$$

$$136 k_{yn} = k_0 n_{\text{sub}} \sin \theta_{mn} \sin \phi_{mn}, \quad (4b)$$

$$137 k_{zmn} = k_0 n_{\text{sub}} \cos \theta_{mn}. \quad (4c)$$

135 as illustrated in Fig. 2(b). Here  $\phi_{mn}$  is the azimuthal angle in the  
136 range  $[0, 2\pi)$ , measured counter-clockwise from the  $k_x$  axis, and  
137  $\theta_{mn}$  in the range  $[0, \pi/2)$  is the propagation angle measured from

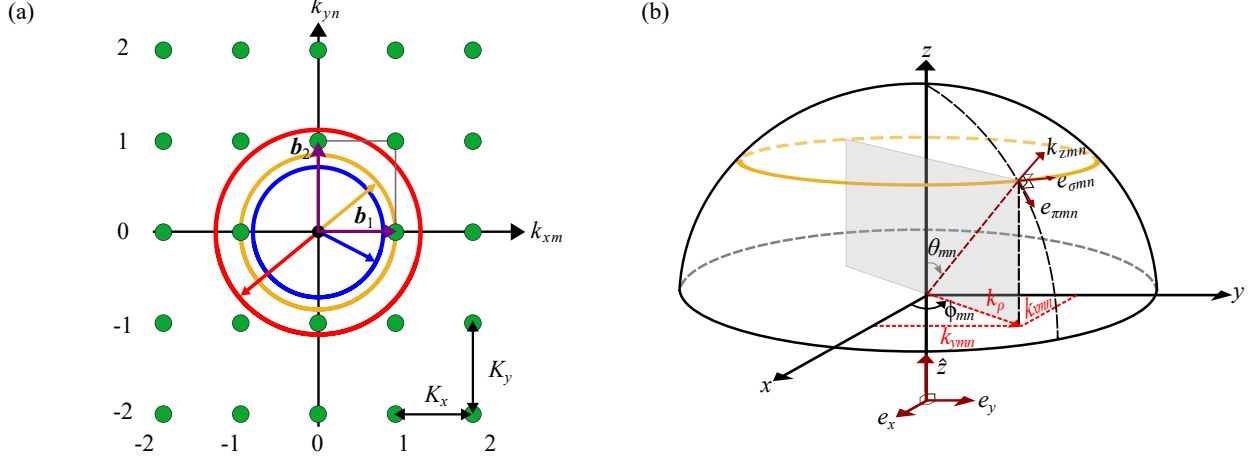


Figure 2: (a) Diffraction orders of a rectangular lattice in spatial-frequency representation at normal incidence. Diffraction orders are represented by dots at positions  $k_{xm} = mK_x$ ,  $k_{yn} = nK_y$ . Blue and red circles represent the cut-off radial spatial frequencies  $k_\rho = k_0 n_{\text{sub}}$  and  $k_\rho = k_0 n_{\text{sup}}$ , respectively, between which BSW excitation is possible. The yellow circle indicates the radial spatial frequency of BSW on a given ML. (b) Definition of the propagation angles ( $\theta_{mn}$ ,  $\phi_{mn}$ ) of a single transmitted diffracted order ( $m, n$ ) in its exit plane (the grey rectangle) and the  $\pi - \sigma$  basis of the diffracted electric field.

138 the  $k_z$  axis. It will prove convenient to use the so-called  $\pi - \sigma$   
 139 basis (or local TM/TE basis) to define the polarization states of the  
 140 transmitted orders. As described in Ref. [21], this basis allows us  
 141 to treat incident fields with any polarization state, including partial  
 142 polarization. Here, however, we are mainly interested in either fully  
 143 polarized or unpolarized illumination.

144 If the incident plane wave is fully polarized, we can use any suit-  
 145 able rigorous grating analysis method (in our case FMM) to deter-  
 146 mine the transverse Cartesian components  $e_{xmn}$  and  $e_{ymn}$  of the  
 147 polarization vector for any transmitted order, as discussed shortly  
 148 below. The longitudinal component of  $e_{mn}$  is fixed by Maxwell's  
 149 divergence equation, which gives  $\mathbf{k}_{mn} \cdot \mathbf{e}_{mn} = 0$  and

$$e_{zmn} = -\frac{1}{k_{zmn}} (k_{xm} e_{xmn} + k_{yn} e_{ymn}). \quad (5)$$

150 In the  $\pi - \sigma$  basis the polarization state of any order is described  
 151 by a two-dimensional vector  $\mathbf{e}_{\pi\sigma mn} = [e_{\pi mn}, e_{\sigma mn}]^T$ , where the  
 152  $\pi$  and  $\sigma$  components are explicitly given by

$$e_{\pi mn} = e_{xmn} \cos \theta_{mn} \cos \phi_{mn} + e_{ymn} \cos \theta_{mn} \sin \phi_{mn} - e_{zmn} \sin \theta_{mn}, \quad (6a)$$

$$e_{\sigma mn} = -e_{xmn} \sin \phi_{mn} + e_{ymn} \cos \phi_{mn}. \quad (6b)$$

153 As shown in Fig. 2(b), the component  $e_{\pi mn}$  lies in the exit plane,  
 154 whereas  $e_{\sigma mn}$  is perpendicular to it. Hence, they represent the TM  
 155 and TE components of the electric field in the exit plane, respec-  
 156 tively.

157 In diffraction by two-dimensionally periodic gratings, the polar-  
 158 ization states of the transmitted (and reflected) diffracted orders  
 159 generally depend on the state of input polarization. We represent  
 160 the polarization vector of a (generally, elliptically polarized) unit-  
 161 amplitude input plane wave as

$$\mathbf{e} = e_x \hat{\mathbf{x}} + e_y \hat{\mathbf{y}} = \hat{\mathbf{x}} \cos \alpha + \hat{\mathbf{y}} \sin \alpha \exp(i\delta), \quad (7)$$

162 normalized such that  $\mathbf{e} = 1$ . The effect of the grating on transmitted  
 163 radiation can be analyzed by calculating (by FMM) the transmis-

164 sion coefficients

$$T_{xmn}^{(x)}, T_{ymn}^{(x)}, T_{xmn}^{(y)}, T_{ymn}^{(y)}, \quad (8)$$

165 for all diffraction orders, where the superscripts  $(x)$  and  $(y)$  re-  
 166 fer to illumination by a purely  $x$ -polarized ( $\mathbf{e} = \hat{\mathbf{x}}$ ) or  $y$ -polarized  
 167 ( $\mathbf{e} = \hat{\mathbf{y}}$ ) incident wave. The coefficients in Eq. (8) are precisely  
 168 the complex vector amplitudes that appear in the Rayleigh plane-  
 169 wave expansion of the field at the output plane of the grating; see,  
 170 e.g., Eq. (5) in Ref. [20]. For an arbitrarily (fully) polarized incident  
 171 wave the transverse electric-field components of the transmitted or-  
 172 ders are [21]

$$e_{xmn} = T_{xmn}^{(x)} e_x + T_{xmn}^{(y)} e_y, \quad (9a)$$

$$e_{ymn} = T_{ymn}^{(x)} e_x + T_{ymn}^{(y)} e_y. \quad (9b)$$

173 The longitudinal components  $e_{zmn}$  are obtained from Eq. (5), and  
 174 the  $\pi - \sigma$  representation of each order is given by Eqs. (6). Since the  
 175 input polarization state affects both the  $\pi$  and  $\sigma$  components, it can  
 176 be used as a design degree of freedom in multiple-BSW excitation,  
 177 in addition to the geometrical grating parameters.

178 It is customary to describe the state of polarization of a fully po-  
 179 larized field by a  $2 \times 2$  polarization matrix  $\mathbf{J} = \mathbf{e}^* \mathbf{e}^T$  (Ref. [22],  
 180 sec. 6.3.2). Explicitly, for the incident field,

$$\mathbf{J} = \begin{bmatrix} J_{xx} & J_{xy} \\ J_{yx} & J_{yy} \end{bmatrix} = \begin{bmatrix} |e_x|^2 & e_x^* e_y \\ e_y^* e_x & |e_y|^2 \end{bmatrix}, \quad (10)$$

181 where the asterisk denotes complex conjugation. Correspondingly,  
 182 the polarization state of any transmitted order in the  $\pi - \sigma$  basis is  
 183 described by  $\mathbf{J}_{\pi\sigma mn} = \mathbf{e}_{\pi\sigma mn}^* \mathbf{e}_{\pi\sigma mn}^T$  [21], explicitly

$$\mathbf{J}_{\pi\sigma mn} = \begin{bmatrix} J_{\pi\pi mn} & J_{\pi\sigma mn} \\ J_{\sigma\pi mn} & J_{\sigma\sigma mn} \end{bmatrix} = \begin{bmatrix} |e_{\pi mn}|^2 & e_{\pi mn}^* e_{\sigma mn} \\ e_{\sigma mn}^* e_{\pi mn} & |e_{\sigma mn}|^2 \end{bmatrix}. \quad (11)$$

184 The polarization states of the diffracted orders can also be charac-  
185 terized by the Stokes parameters [21]

$$S_{0mn} = J_{\pi\pi mn} + J_{\sigma\sigma mn}, \quad (12a)$$

$$S_{1mn} = J_{\pi\pi mn} - J_{\sigma\sigma mn}, \quad (12b)$$

$$S_{2mn} = 2\Re(J_{\pi\sigma mn}), \quad (12c)$$

$$S_{3mn} = 2\Im(J_{\pi\sigma mn}), \quad (12d)$$

186 where  $\Re$  and  $\Im$  denote the real and imaginary parts. The nor-  
187 malized forms of the Stokes parameters are defined as  $s_{jmn} =$   
188  $S_{jmn}/S_{0mn}$  ( $j = 1, 2, 3$ ), and the degree of polarization associ-  
189 ated with order  $(m, n)$  is given by

$$P_{mn} = \sqrt{s_{1mn}^2 + s_{2mn}^2 + s_{3mn}^2}. \quad (13)$$

190 For a fully polarized incident wave,  $P_{mn} = 1$  for all orders, even  
191 though the values of the individual Stokes parameters generally de-  
192 pend on order indices.

193 In addition to fully polarized illumination, we consider the opposite  
194 extreme case of unpolarized illumination. The matrix  $\mathbf{J}$  for partially  
195 polarized light is defined as  $\mathbf{J} = \langle e^* e^T \rangle$ , where the brackets denote  
196 ensemble averaging over all polarization realizations. For unpolar-  
197 ized illumination it has a diagonal form (Ref. [22], sec. 6.3.3)

$$\mathbf{J} = \frac{1}{2} \begin{bmatrix} 1 & 0 \\ 0 & 1 \end{bmatrix} \quad (14)$$

198 and the degree of input polarization is  $P = 0$ . The polarization ma-  
199 trix associated with order  $(m, n)$  can be represented as an average

$$\mathbf{J}_{\pi\sigma mn} = \frac{1}{2} \left[ \mathbf{J}_{\pi\sigma mn}^{(x)} + \mathbf{J}_{\pi\sigma mn}^{(y)} \right], \quad (15)$$

200 which remains diagonal because  $e_x$  and  $e_y$  are uncorrelated. How-  
201 ever, since the grating treats these components differently, in gen-  
202 eral  $J_{\pi\pi mn} \neq J_{\sigma\sigma mn}$ , implying that the individual orders become  
203 partially polarized with  $P_{mn} > 0$ .

204 In standard beam splitting problems in resonance-domain diffrac-  
205 tive optics [20] one is interested in the distribution of the diffraction  
206 efficiencies of the propagating orders. Since we have normalized  
207 the intensity of the incident field such that  $S_0 = 1$ , the diffraction  
208 efficiencies are defined as [21]

$$\eta_{mn} = n_{\text{sub}} \cos \theta_{mn} S_{0mn}. \quad (16)$$

209 **In BSW excitation problem, the design goal is to maximize and**  
210 **equalize the coupling of the incident field to a set of BSW modes**  
211 **with the angle  $\theta_{mn}$  equal to  $\theta_{\text{BSW}}$ . If  $\theta_{\text{BSW}}$  is the excitation angle**  
212 **for TE polarization, the component  $e_{\sigma mn}$  excites a BSW while**  
213  **$e_{\pi mn}$  is non-resonant, and vice versa.**

214 We choose the geometry such that several diffraction orders have  
215 the same radial spatial frequency  $k_{\rho mn} = k_0 n_{\text{sub}} \sin \theta_{\text{BSW}}$ , and  
216 therefore lie on the yellow circle depicted in Fig. 2(a). The relative  
217 amplitudes of the excited BSWs are determined by the  $\sigma$ -polarized

218 components  $J_{\sigma\sigma mn}$  in TE polarization and  $J_{\pi\pi mn}$  in TM polar-  
219 ization. The fraction

$$\kappa_{mn} = J_{\sigma\sigma mn} / J_{\pi\pi mn} \quad (17)$$

220 provides the ratio of the coupled and uncoupled parts of the inci-  
221 dent wave in BSW excitation.

## 222 4 Plane-wave design with linear gratings

223 As evident from the preceding discussion, the  $\pi - \sigma$  representation  
224 returns the BSW excitation problem to the basic TE or TM polar-  
225 ized problem. In addition, since we assume a substrate thickness  
226  $H \gg \lambda_0$ , the evanescent parts of the diffracted fields above the  
227 grating and the BSW field below the stack are spatially well sepa-  
228 rated. Hence, we may treat the BSW stack design and the grating  
229 design as two separate problems. In order to obtain an illustrative  
230 stack design useful for our purposes, we fix  $\lambda_0 = 514$  nm and pro-  
231 vide a stack geometry sustaining BSWs at angles between the blue  
232 and red lines in Fig. 2(a). The resulting stack can then be used to  
233 design gratings for excitation of BSWs that lie on the yellow circle  
234 in Fig. 2(a).

235

### 236 4.1 Multilayer stack design

237 Figure 3(a) shows the assumed stack structure, which consists of  
238  $N$  high/low (H/L) refractive index bilayers and a terminating top  
239 (T) layer with refractive indices  $n_{\text{H}}$ ,  $n_{\text{L}}$ ,  $n_{\text{T}}$  and thicknesses  $h_{\text{H}}$ ,  
240  $h_{\text{L}}$ ,  $h_{\text{T}}$ , respectively. To reduce the number of variable parameters,  
241 we consider TE polarization, fix the number of bilayers to  $N = 6$ ,  
242 use refractive indices  $n_{\text{H}} = 2.520$  (TiO<sub>2</sub>),  $n_{\text{L}} = 1.476$  (SiO<sub>2</sub>),  
243  $n_{\text{T}} = n_{\text{H}} = 2.520$ . The thicknesses  $h_{\text{H}}$ ,  $h_{\text{L}}$ ,  $h_{\text{T}}$  are used to design  
244 the stack such that the BSW resonance occurs at an angle  $\theta_{mn}$  in  
245 the exit plane.

246 Figure 3(b) shows the design results. The horizontal axis is  
247  $k_x/k_0 = n_{\text{sub}} \sin \theta_{mn} = n_{\text{eff}}$ , where  $n_{\text{eff}}$  can be interpreted as  
248 the effective index of the stack. The plotting range starts from the  
249 critical angle of BSW generation and extends to  $k_x/k_0 n_{\text{sub}}$ , i.e., it  
250 spans the region between the blue and red circles in Fig. 2(a). As  
251  $n_{\text{eff}}$  increases, the BSW becomes increasingly buried within the  
252 multilayer and acts less like a surface mode. At the same time, all  
253 layer thicknesses show a monotonically increasing trend.

254

### 255 4.2 Two-way splitting

256 As illustrated in Fig. 1, the coupling of two counter-propagating  
257 BSWs is possible with linear gratings ( $d_x = d$ ,  $d_y = \infty$ ). The  
258 exit plane of both orders,  $(m, n) = (-1, 0)$  and  $(+1, 0)$ , is the  $xz$   
259 plane and the  $\pi - \sigma$  representation reduces to the standard TM/TE

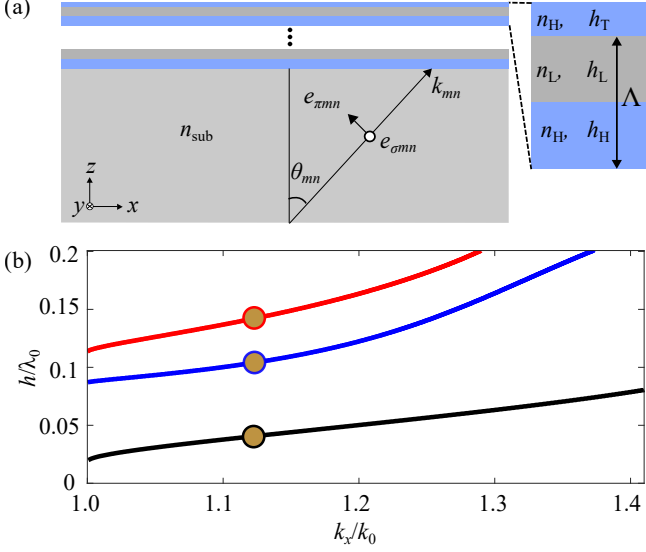


Figure 3: (a) Definition of the multilayer structure and notation. (b) Stack parameters as a function of the ratio  $k_x/k_0 = n_{\text{eff}}$  for TE-mode BSW excitation with  $N = 6$  bilayers:  $h_H/\lambda_0$  (blue),  $h_L/\lambda_0$  (red), and  $h_T/\lambda_0$  (black). The dots mark the position  $k_x/k_0 = 1.1209$  for BSW excitation at  $50^\circ$  angle of incidence.

decomposition. Since, by symmetry,  $\eta_{-1,0} = \eta_{+1,0}$  for binary profiles defined in the inset of Fig. 1, we need to maximize  $\eta_{+1,0}$ . This also leads to the optimum value of  $J_{\sigma\sigma mn}$ , while  $J_{\pi\pi mn} = 0$ . Now we only need to find the values of the fill factor  $f = c/\lambda_0$  and grating height  $h/\lambda_0$  that maximize  $\eta_{+1,0}$  ( $= \eta_{-1,0}$ ) to also maximize  $J_{\sigma\sigma}$ .

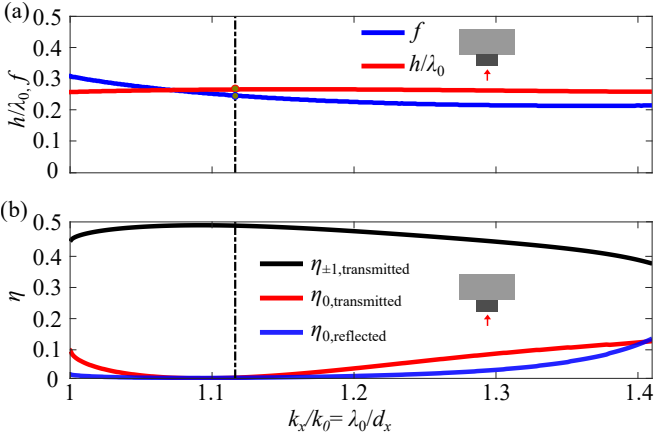


Figure 4: Design of two-way beam splitters. (a) Optimum values of the fill factor  $f$  (red) and the relief depth  $h/\lambda_0$  (blue) as a function of the exit angle of the first diffracted order in TE polarization. (b) The corresponding first-order diffraction efficiency  $\eta_{+1,0} = \eta_{-1,0}$  (black), the efficiency  $\eta_{0,0}$  of the zeroth transmitted order (red), and that of the zeroth reflected order (blue), which is  $1 - 2\eta_{+1,0} - \eta_{0,0}$  due to energy conservation. The inset shows the grating structure and direction of illumination.

The grating-design results are summarized in Fig. 4(a). The optimum fill factor remains fairly constant over the entire angular range considered here, whereas the optimum grating height decreases with increasing angle. The efficiencies of all propagating orders are plotted in Fig. 4(b). At around  $k_x/k_0 = 1.1209$  (corresponding to an excitation angle  $50^\circ$ ) we get  $\eta_{\pm 1,0} \approx 0.4973$ . Some

light is ‘lost’ in zeroth reflected and transmitted orders when we move close to the cut-off at  $k_x/k_0 = 1$  or towards larger values of  $k_x/k_0$ , but the designs remain acceptable over a relatively wide range of excitation angles.

The results in Figs. 3(b) and 4 allow us to design two-way beam splitters for any BSW resonance angle of interest. The stack design for the desired angle is obtained from Fig. 3(b) and the corresponding grating design from Fig. 4(a). The performance of the design can be evaluated from Fig. 4(b). To limit the number of variables further, we set  $\theta_{\text{BSW}} = 50^\circ$ , corresponding to  $k_x/k_0 = 1.1209$ . The stack design is marked by the dots in Fig. 3(b), the optimum parameters for TE excitation with  $N = 6$  bilayers being  $h_H = 60$  nm,  $h_L = 85$  nm, and  $h_T = 20$  nm. Correspondingly, the vertical lines in Fig. 4(a) give a grating design  $f = 0.2536$ ,  $h/\lambda_0 = 0.2752$ , with  $\eta_{\pm 1,0} = 0.4973$ .

Considering the optimized case represented by the dots on Fig. 3 and the black dashed line on Fig. 4, simulation of the reflected and transmitted coefficients has been performed for the full structure. It implies a grating of period  $d \simeq 459$  nm and fill factor is  $f = 0.2536$  and  $h/\lambda_0 = 0.2752$  on the lower side of a  $10\text{-}\mu\text{m}$ -thick fused silica wafer on top of which the multilayer is deposited. The multilayer design leads to a Bloch surface wave excited when the first diffracted order emerge from the grating at an angle of  $50^\circ$  ( $k_x/k_0 = 1.1209$ ) at a wavelength of 514 nm. This is observed in Fig. 5(a), where a strong dip in reflection arises at this value of  $k_x/k_0$ . In Fig. 5(b) the response in wavelength is presented. One can observe a relatively strong peak in transmission slightly shifted with regards to the reflection dip.

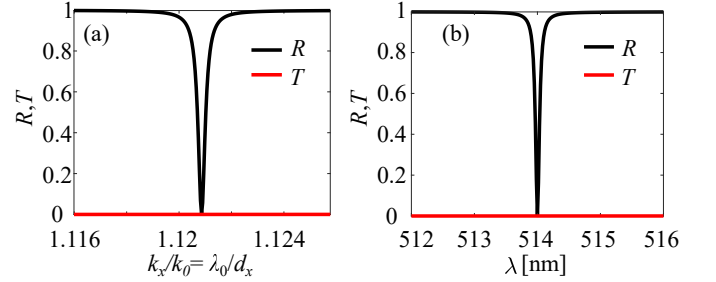


Figure 5: Response of the full structure (grating, substrate, multilayer and superstrate). (a) and (b) Reflected (black curves) and transmitted (red curves) first diffracted orders as a function of the normalized wavevector (a) and wavelength (b).

## 5 Plane-wave design with biperiodic gratings

We proceed to design of two-dimensionally periodic gratings that allow simultaneous excitation of more than two BSWs. Two lattice geometries are considered: square lattices for four-way excitation and hexagonal lattices for six-way excitation.

## 307 5.1 Four-way splitting

308 Let us first consider biperiodic gratings with primitive direct-  
 309 lattice vectors  $\mathbf{a}_1 = d\hat{x}$ ,  $\mathbf{a}_2 = d\hat{y}$ . The (Wigner–Seitz) primi-  
 310 tive cell is square-shaped, covering the area  $-d/2 < x < d/2$ ,  
 311  $-d/2 < y < d/2$ . The spatial frequencies of the diffraction or-  
 312 ders are then  $k_{xm} = mK$ ,  $k_{yn} = nK$ , the coordination number  
 313 is 4, and the nearest neighbors of the zeroth order  $(0, 0)$ , namely  
 314  $(m, n) = (+1, 0)$ ,  $(0, +1)$ ,  $(-1, 0)$ ,  $(0, -1)$ , propagate in direc-  
 315 tions  $\phi_{+1,0} = 0$ ,  $\phi_{0,+1} = \pi/2$ ,  $\phi_{-1,0} = \pi$ ,  $\phi_{0,-1} = 3\pi/2$ , re-  
 316 spectively. By an appropriate choice of  $d$ , all of these four orders  
 317 can be placed simultaneously on the yellow ring in Fig. 2(a), thus  
 318 enabling four-way BSW excitation.

319 In the design, we found it sufficient to consider binary ( $z$ -invariant)  
 320 relative-permittivity profiles of the particular form

$$\epsilon_r(x, y, z) = \begin{cases} n_1^2 & \text{when } x^2 + y^2 < r^2 \\ n_2^2 & \text{otherwise} \end{cases} \quad (18)$$

321 in  $0 < z < h$  within the primitive cell. The circular feature defined  
 322 by the radius  $r$  can be either a pillar ( $n_1 = n_{\text{sub}}$ ,  $n_2 = 1$  or a  
 323 hole ( $n_1 = 1$ ,  $n_2 = n_{\text{sub}}$ ) etched in the substrate. This type of pil-  
 324 lar/hole structures can be patterned at a nanometer-scale addressing  
 325 resolution using electron beam lithography system available to us,  
 326 and require only a single etching step.

327 The radius  $r$  and the relief depth  $h$  can be used as the structural  
 328 design parameters. Some symmetry rules exist, which are helpful  
 329 in the design. Since the unit cell and the structure are centered at the  
 330 origin, the transmission coefficients in Eq. (8) satisfy the inversion  
 331 symmetry rules

$$T_{x,-m,-n} = T_{xmn}, \quad T_{y,-m,-n} = T_{ymn}, \quad (19)$$

332 for both ( $x$ ) and ( $y$ ) input polarizations. These rules hold regard-  
 333 less of the input polarization state, which however has an effect on  
 334 the actual values of  $T_{xmn}$  and  $T_{ymn}$ . They reduce the number of  
 335 orders that we need to (or can) control from four to two: we see  
 336 from Eq. (19) that  $\eta_{-m,-n} = \eta_{mn}$ . Similar symmetry rules hold  
 337 also for  $J_{\sigma\sigma mn}$  and  $J_{\pi\pi mn}$ .

338 We begin the design of four-way couplers by optimizing the struc-  
 339 tural parameters  $r$  and  $h$  to minimize the sum of the efficiencies  
 340 of the reflected and transmitted zeroth orders. This maximizes the  
 341 combined efficiency of the four nearest-neighbor diffraction orders,  
 342 and leaves the polarization state of the incident field free for design.  
 343 Choosing  $\theta_{\text{BSW}} = 50^\circ$  ( $d \approx 0.892\lambda_0$ ), for either  $45^\circ$  or circu-  
 344 larly polarized illumination and considering pillars, we get a design  
 345  $r \approx 0.201\lambda_0$ ,  $h \approx 0.53176\lambda_0$ , which gives reflected and transmit-  
 346 ted zero-order efficiencies of  $\sim 3.5\%$  and  $\sim 5.2\%$ , respectively,  
 347 leaving the rest of the incident energy to be distributed among the  
 348 nearest-neighbor orders.

349 Our remaining target is to equalize (and maximize) the coupling  
 350 strengths  $J_{\sigma\sigma mn}$  of the four signal orders by designing the input  
 351 polarization state defined in Eq. (7). The symmetry in the 4-way

352 splitting implies that there is no structurally induced polarization  
 353 conversion: for ( $x$ )-polarized input we get  $J_{\sigma\sigma mn} = 0$  for orders  
 354  $(m, n) = (\pm 1, 0)$ , while ( $y$ )-polarized input gives  $J_{\sigma\sigma mn} = 0$   
 355 for orders  $(m, n) = (0, \pm 1)$ . Considering linearly polarized light,  
 356 the values of  $J_{\sigma\sigma mn}$  (and  $J_{\pi\pi mn}$ ) vary rapidly with the angle  $\alpha$ .  
 357 Choosing  $\alpha \approx \pi/4$  gives values  $J_{\sigma\sigma mn} \approx 0.063$  and  $\kappa_{mn} \approx 0.359$   
 358 for all four orders. The same result is obtained also for circularly  
 359 polarized illumination with  $\alpha \approx \pi/4$ ,  $\delta = \pm\pi/2$ . Both the opti-  
 360 mized diffracted efficiencies and the maximized coupling strengths  
 361 occur at the same illumination polarization.

362 Considering unpolarized illumination, the matrix  $\mathbf{J}_{\pi\sigma mn}$  becomes  
 363 diagonal and the degree of polarization takes the form

$$P_{mn} = |s_{1mn}| = \frac{|J_{\pi\pi mn} - J_{\sigma\sigma mn}|}{J_{\pi\pi mn} + J_{\sigma\sigma mn}}. \quad (20)$$

364 With the present numerical values we obtain  $P_{mn} \approx 0.473$  for all  
 365 nearest-neighbor orders. Even though the excitation wave is parti-  
 366 tially polarized, we obtain the same values of  $J_{\sigma\sigma mn}$  as above;  
 367 both of the two mutually uncorrelated components of the incident  
 368 field contribute to TE-mode BSW excitation.

## 370 5.2 Six-way splitting

371 Let us consider a grating with hexagonal symmetry, which allows  
 372 simultaneous excitation of six BSWs. The primitive vectors are  
 373 now  $\mathbf{a}_1 = d\hat{x}$  and  $\mathbf{a}_2 = (d/2)\hat{x} + (\sqrt{3}d/2)\hat{y}$ , and the Wigner–  
 374 Seitz primitive cell is a hexagon as shown in Fig. 6(a). It will,  
 375 however, be convenient for our purposes to define a rectangular  
 376 direct-lattice cell as in Ref. [20], which covers the spatial region  
 377  $-d/2 < x < d/2$ ,  $-\sqrt{3}d/2 < y < \sqrt{3}d/2$  in Fig. 6(a). This  
 378 alternative lattice representation simplifies the visualization of the  
 379 geometry. It also allows the use of FMM in a cartesian instead of  
 380 a non-orthogonal basis, as in Ref. [20], though in the present work  
 381 we actually used the latter basis.

382 The spatial-frequency structure defined by the reciprocal-lattice  
 383 primitive vectors  $\mathbf{b}_1 = K\hat{x} - (K/\sqrt{3})\hat{y}$ ,  $\mathbf{b}_2 = (2K/\sqrt{3})\hat{y}$  with  
 384  $K = 2\pi/d$  is illustrated in Fig. 6(b), where the solid green circles  
 385 show the locations of the allowed orders in the cartesian  $(k_x, k_y)$   
 386 system. The empty circles represent the orders of the rectangular  
 387 spatial lattice, which are forbidden by the hexagonal symmetry.  
 388 The yellow circle connects the six nearest neighbors of the ze-  
 389 roth order that satisfy the condition for BSW excitation simulta-  
 390 neously: orders  $(m, n) = (+1, +1)$ ,  $(0, +2)$ ,  $(-1, +1)$ ,  $(-1, -1)$ ,  
 391  $(0, -2)$ ,  $(+1, -1)$  of the rectangular lattice, with exit planes at an-  
 392 gles  $\pi/6 + q\pi/3$ ,  $q = 0, \dots, 5$ . The excited BSWs propagate along  
 393 the surface of the stack in these directions.

394 In hexagonal lattice geometry, the symmetry rules in Eq. (19) en-  
 395 sure  $J_{\sigma\sigma,-1,-1} = J_{\sigma\sigma,1,1}$ ,  $J_{\sigma\sigma,0,-2} = J_{\sigma\sigma,0,2}$ ,  $J_{\sigma\sigma,-1,1} =$   
 396  $J_{\sigma\sigma,1,-1}$ . These symmetries leave us three pairs of orders to con-  
 397 trol, and we expect to need additional structural freedom compared  
 398 to the 4-wave case. Let us nevertheless see what designs are pos-

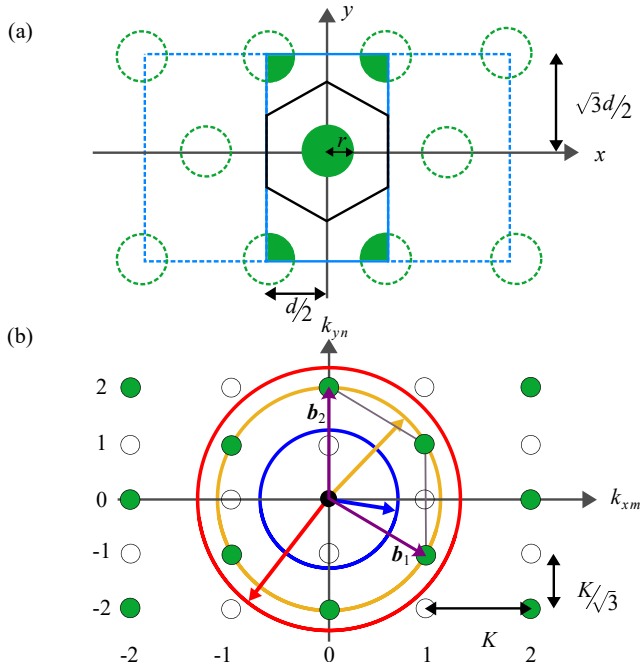


Figure 6: (a) The spatial structure of a hexagonal grating. The hexagon shows the spatial Wigner-Seitz primitive cell, the green features illustrate the grating structure, and the blue rectangle shows the non-primitive cartesian cell. (b) The spatial-frequency grid. The filled and empty dots represent the allowed and forbidden orders of the hexagonal lattice. The blue, yellow, and red circles have the same meaning as in Fig. 2(a).

399 sible with circular pillars by following the same strategy as above.  
 400 An important difference is that in the hexagonal geometry we do  
 401 have structurally induced polarization conversion.

402 By optimizing  $r$  and  $h$  for pillars, we get  $h \approx 0.422\lambda_0$  and  
 403  $r \approx 0.254\lambda_0$ , which leaves a combined efficiency of  $\sim 0.884$   
 404 available for the 6 orders of interest. The distribution of  $J_{\sigma\sigma mn}$   
 405 again depends on input polarization. We found that it is not possi-  
 406 ble to equalize the coupling exactly for all six orders, but using  
 407 circularly polarized light with  $\alpha = \pi/4$  and  $\delta = 0.486\pi$  we have  
 408  $J_{\sigma\sigma,1,1} = 0.097$ ,  $J_{\sigma\sigma,0,2} = 0.102$ , and  $J_{\sigma\sigma,1,-1} = 0.113$ , respec-  
 409 tively. Similarly, for  $\kappa_{mn}$ , we have  $\kappa_{1,1} = 1.691$ ,  $\kappa_{0,2} = 1.903$ ,  
 410 and  $\kappa_{1,-1} = 2.310$ . Though it is not of concern for the present  
 411 purposes, it is worth noting that the diffraction efficiencies are:  
 412  $\eta_{1,1} \approx 0.152$ ,  $\eta_{0,2} \approx 0.145$ , and  $\eta_{1,-1} \approx 0.144$ . As with the  
 413 four-wave case, the design with circular pillars works also for cir-  
 414 cularly polarized or unpolarized illumination but the exact values  
 415 of  $J_{\sigma\sigma mn}$  depend on polarization, but are within the same range as  
 416 above. For unpolarized illumination, the degrees of polarization of  
 417 the individual orders are nearly equal,  $P_{mn} \approx 0.3226$ .

418 In Fig. 7, we show the field amplitude distribution associated with  
 419 the six-way coupling geometry in the  $xz$ -plane, i.e., crossing the  
 420 multilayer, when illuminated with a  $45^\circ$  polarized light wave.  
 421 The field is evaluated over 3-unit cells, i.e., 3 grating periods, in  
 422 the  $x$ -direction. It shows, as expected, a strong field on the upper  
 423 medium, which such structure ideal for sensing applications, espe-

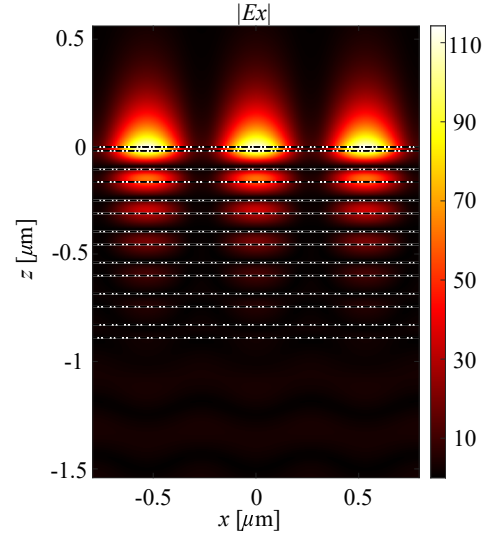


Figure 7: Field amplitude distribution across the multilayer ( $xz$ -plane). The illumination polarization was set to  $45^\circ$ . The dashed lines superimposed on the field represent the multilayer interfaces.

424 cially when providing multiple sensing areas thanks to the splitting  
 425 of the BSW excitation.

## 426 6 Discussion

427 Throughout the paper we have considered normally incident illu-  
 428 mination. The use of non-normal incidence could potentially allow  
 429 us to consider other combinations of diffracted orders being simul-  
 430 taneously resonant. Changing the angle of incidence moves the grid  
 431 of diffracted orders transversely in Fig. 2(a) with respect to the cir-  
 432 cles centered at the origin. For instance, if the propagation direction  
 433 of the incident field is chosen as  $(k_{x1}, k_{y1}) = (0, k_{y1})$ , increasing  
 434  $k_{y1}$  moves the grid downwards in  $k_y$  direction, giving the orders at  
 435 positions  $k_{xm} = mK_x$ ,  $k_{yn} = k_{y1} + nK_y$ . Hence the three orders  
 436  $(m, n) = (0, 0)$  and  $(m, n) = (\pm 1, 0)$  would have a common ra-  
 437 dial spatial frequency if  $k_{y1} = -(K_x^2 + K_y^2)/2K_y$ , being therefore  
 438 available for 3-way BSW excitation. To avoid order  $(0, 2)$  from oc-  
 439 cupping the same ring as the zeroth order, we would need to choose  
 440  $K_x \neq K_y$ . However, placing the (yellow) BSW resonance ring out-  
 441 side the blue ring in Fig. 2(a) requires  $k_{\rho 00} > k_0 n_{\text{sub}}$ , which is not  
 442 possible with incidence from air. Hence a Kretschmann excitation  
 443 geometry would be needed, thus sacrificing the compact footprint  
 444 of the setup.

445 As an alternative to the geometry considered in this paper, we could  
 446 consider having the splitter grating and the BSW stack as an inte-  
 447 grated structure. This would still allow a compact platform at nor-  
 448 mal incidence, but the grating design and BSW stack design would  
 449 not be independent anymore. As a first drawback, the splitter grat-  
 450 ing would most likely have to be rather thick ( $\sim \lambda_0$ ) to suppress  
 451 the zeroth transmitted order, preventing the possibility of etching it  
 452 in the top ML layer. As a consequence, a strong degrading effect  
 453 in the excited BSWs would be expected. Alternatively, one could  
 454 use a highly index-modulated splitter grating with a flat top sur-  
 455 face immediate below the stack. This would partially alleviate the

456 dependency in the ML and the grating design, but presumably the  
457 BSWs would be less affected.

## 458 7 Conclusions

459 In summary, we considered grating design for 2-way, 4-way, and  
460 6-way BSW coupling at normally incident but arbitrarily polarized  
461 illumination of gratings with linear, square, and hexagonal symme-  
462 tries. The plane-wave designs feature ideal TE-mode BSW cou-  
463 pling in the two-wave case. In the other cases the non-resonant  
464 parts of the excitation orders cannot be eliminated simultaneously,  
465 and they actually dominate the resonant ( $\sigma$  polarized) parts by a  
466 factor of  $\sim 2.8$  in the 4-wave case. The 6-wave case reveals the  
467 opposite observation with the resonant part dominating by a factor  
468 of  $\sim 1.968$  making them ideal candidate for TE-mode BSW exci-  
469 tation. Nevertheless, in the 4-wave case all four coupling ratios can  
470 be made equal, and in the 6-wave case practically equal, for several  
471 input polarization states of practical significance.

## 472 Funding

473 The work was partially funded by the Academy of Finland through  
474 project 333938 and the Flagship Program PREIN (346518). E. De-  
475 scrovi acknowledges the funding received by Italian “Ministero  
476 dell’Università e della Ricerca” under the “Dipartimento di Eccel-  
477 lenza 2018-2022” program.

## 478 Disclosures

479 The authors declare no conflicts of interest.

## 480 REFERENCES

481 [1] W. M. Robertson, M. S. May, “Surface electromagnetic  
482 wave excitation on one-dimensional photonic band-gap  
483 arrays,” *Appl. Phys. Lett.* **74**, 1800–1802 (1999).  
484 [2] M. Liscidini, J. E. Sipe, “Enhancement of diffraction for  
485 biosensing applications via Bloch surface waves,” *Appl.*  
486 *Phys. Lett.* **91**, 253125 (2007).  
487 [3] F. Villa and J. A. Gaspar-Armenta, “Photonic crystal to  
488 photonic crystal surface modes: narrow-bandpass filters,”  
489 *Opt. Express* **12**, 2338–2355 (2004).  
490 [4] E. Mogni, G. Pellegrini, J. Gil-Rostra, F. Yubero, G. Si-  
491 mone, S. Fossati, J. Dostálek, R. Martínez Vázquez, R.  
492 Osellame, M. Celebrano, M. Finazzi, P. Biagioni, “One-  
493 dimensional photonic crystal for surface mode polariza-  
494 tion control,” *Adv. Opt. Mater.* 2200759 (2022).  
495 [5] A. L. Asilevi, H. Pesonen, S. Pelisset, E. Descrovi,  
496 M. Roussey, and J. Turunen, “Pulse modulation by

497 Bloch Surface Wave excitation,” *Opt. Lett.* **47**, 2574–2577  
498 (2022).

499 [6] E. Descrovi, F. Frascella, B. Sciacca, F. Geobaldo, L.  
500 Dominici, F. Michelotti, “Coupling of surface waves in  
501 highly defined one-dimensional porous silicon photonic  
502 crystals for gas sensing applications,” *Appl. Phys. Lett.*  
503 **91**, 241109 (2007).  
504 [7] D. N. Gulkin, A. A. Popkova, B. I. Afinogenov, D. A.  
505 Shilkin, K. Kuršelis, B. N. Chichkov, V. O. Bessonov,  
506 A. A. Fedyanin, “Mie-driven directional nanocoupler for  
507 Bloch surface wave photonic platform,” *Nanophotonics*  
508 **10**, 2939–2947 (2021).  
509 [8] M. Wang, H. Zhang, T. Kovalevich, R. Salut, M.-S. Kim,  
510 M. A. Suarez, M.-P. Bernal, H.-P. Herzig, H. Lu, T. Gros-  
511 jean, “Magnetic spin-orbit interaction of light,” *Light Sci.*  
512 *Appl.* **7**, 24 (2018).  
513 [9] R. Wang, H. Xia, D. Zhang, J. Chen, L. Zhu, Y. Wang, E.  
514 Yang, T. Zang, Tianyang, X. Xiaolei, G. Zou, P. Wang, H.  
515 Ming, R. Badugu, J. R. Lakowicz, “Bloch surface waves  
516 confined in one dimension with a single polymeric nanofi-  
517 bre,” *Nat. Commun.* **8**, 14330 (2017).  
518 [10] K. R. Safronov, V. O. Bessonov, D. V. Akhremenkov, M.  
519 A. Sirotin, M. N. Romodina, E. V. Lyubin, I. V. Sobol-  
520 eva, A. A. Fedyanin, “Miniature Otto prism coupler for  
521 integrated photonics,” *Laser & Photonics Reviews*, **16**,  
522 2100542 (2022).  
523 [11] E. A. Bezus, D. A. Bykov, L. L. Doskolovich, “Integrated  
524 diffraction gratings on the Bloch surface wave platform  
525 supporting bound states in the continuum,” *Nanopho-*  
526 *tonics* **10**, 4331–4340 (2021).  
527 [12] T. Kovalevich, P. Boyer, M. Suarez, R. Salut, M.-S.  
528 Kim, H. P. Herzig, M.-P. Bernal, T. Grosjean, “Polariza-  
529 tion controlled directional propagation of Bloch surface  
530 wave,” *Opt. Express* **25**, 5710 (2017).  
531 [13] M. Scaravilli, A. Micco, G. Castaldi, G. Coppola, M.  
532 Giofrè, M. Iodice, V. La Ferrara, V. Galdi, A. Cusano,  
533 “Excitation of Bloch surface waves on an optical fiber  
534 tip,” *Adv. Opt. Mater.* **6**, 1800477 (2018).  
535 [14] V. Koju, W. M. Robertson, “Leaky Bloch-like surface  
536 waves in the radiation-continuum for sensitivity en-  
537 hanced biosensors via azimuthal interrogation,” *Sci. Rep.*  
538 **7**, 3233 (2017).  
539 [15] M. Scaravilli, G. Castaldi, A. Cusano, V. Galdi, “Grating-  
540 coupling-based excitation of Bloch surface waves for lab-  
541 on-fiber optodes,” *Opt. Express* **24**, 27771 (2016).  
542 [16] R. Wang, X. Lei, Y. Jin, X. Wen, L. Du, A. Wu, A. V.  
543 Zayats, X. Yuan, “Directional imbalance of Bloch sur-  
544 face waves for ultrasensitive displacement metrology,”  
545 *Nanoscale* **13**, 11041–11050 (2021).  
546 [17] C.-Z. Deng, Y.-L. Ho, H. Yamahara, H. Tabata, J.-J. De-  
547 launay, “Near-Zero-Index Slabs on Bloch Surface Wave  
548 Platform for Long-Range Directional Couplers and Op-  
549 tical Logic Gates,” *ACS Nano* **16**, 2224–2232 (2022).  
550 [18] X. Lei, R. Wang, L. Liu, C. Xu, A. Wu, Q. Zhan, “Mul-  
551 tifunctional on-chip directional coupler for spectral and  
552 polarimetric routing of Bloch surface wave,” *Nanopho-*

- 553 tonics, doi:10.1515/nanoph-2022-0397 (2022).
- 554 [19] H. Kim, J. Park, and B. Lee, *Fourier Modal Method and*  
555 *its Applications in Computational Nanophotonics* (CRC  
556 Press, 2012).
- 557 [20] E. Noponen and J. Turunen, “Eigenmode method for  
558 electromagnetic synthesis of diffractive elements with  
559 three-dimensional profiles,” *J. Opt. Soc. Am. A* **11**, 2494–  
560 2502 (1994).
- 561 [21] J. Tervo, I. A. Turunen, and B. Bai, “A general approach  
562 to the analysis and description of partially polarized light  
563 in rigorous grating theory,” *J. Eur. Opt. Soc: Rapid Publ.*  
564 **3**, 08004 (2008).
- 565 [22] L. Mandel and E. Wolf, *Optical Coherence and Quantum*  
566 *Optics* (Cambridge, 1995).
- 567 [23] K. R. Safronov, D. N. Gulkin, I. M. Antropov, K.  
568 A. Abrashitova, V O. Bessonov, and A. A. Fedyanin,  
569 “Multimode interference of Bloch surface electromagnetic  
570 waves,” *ACS Nano* **14**, 10428–10437 (2020).
- 571 [24] R. Dubey, B. V. Lahijani, E. Barakat, M. Häyrynen, M.  
572 Roussey, M. Kuittinen, H. P. Herzig, “Near-field char-  
573 acterization of a Bloch-surface-wave-based 2D disk res-  
574 onator,” *Opt. lett.* **41**, 4867–4870 (2016).